DEFORMATION MONITORING USING SAR INTERFEROMETRY AND ACTIVE AND PASSIVE REFLECTORS

M. Crosetto [1, *], G. Luzi [1], O. Monserrat [1], A. Barra [1], M. Cuevas-González [1], R. Palamá [1], V. Krishnakumar [1], Y. Wassie [1], S. M. Mirmazloumi [1], P. Espín-López [1], B. Crippa [2]

[1] Centre Tecnològic de Telecomunicacions de Catalunya, Division of Geomatics, Av. Gauss, 7 E-08860 Castelldefels (Spain) - mcrosetto@cttc.cat
[2] Department of Earth Sciences, Section of Geophysics, University of Milan, Via Cicognara 7, I-20129, Milan, Italy - bruno.crippa@unimi.it

Commission III, WG III/3

KEY WORDS: Deformation, monitoring, SAR, passive reflectors, active reflectors

ABSTRACT:

This paper is focused on SAR interferometry for deformation monitoring, based on the use of passive and active reflectors. Such reflectors are needed in all cases where a sufficient response from the ground is not available. In particular, the paper describes the development of a low-cost active reflector. This development was carried out in an EU H2020 project called GIMS. The paper summarizes the key characteristics of the developed active reflector. The reflector was tested in two main experiments: the first one located in the campus of CTTC and the second one in a GIMS test site located in Slovenia. The experiments demonstrate the visibility of the active reflectors and provide the first results concerning the phase stability of such devices.

1. INTRODUCTION

The success of SAR interferometry highly depends on the presence of good visible targets in the area to be imaged by the radar sensors (Bamler and Hartl, 1998; Rosen et al., 2000; Hanssen, 2001). Such targets provide good phase stability for interferometric applications. In urban and densely populated areas, buildings and infrastructures are available as "natural" good reflectors, while in vegetated areas installation of artificial reflectors called Passive Corner Reflectors (PCR) and Active Reflectors (AR) is key to achieve a good response. The latter one is the more advanced solution. A case study based on PCRs is described in Crosetto et al. (2013).

A PCR is a passive target with a simple geometrical shape, designed to perform a high radar reflectivity. Such objects are usually constructed with metal plates of a size larger than the wavelength, and with faces oriented toward the radar to maximize the energy reflected back to the radar. Several kinds of PCRs can be realized, the one with Triangular Trihedral geometry, see Garthwaite (2017), being the most widely used. PCRs are usually cumbersome to deploy, heavy and affected by heavy weather conditions, like severe rainfall, strong winds and snowfalls. Besides, the installation of a PCR can be difficult due to hard accessibility, e.g. in landslides, glaciers, etc.

An alternative approach is the installation of ARs, which are smaller and lighter. ARs provide a persistent response as a "good target" for amplitude and phase data interpretation. The need of a power source, which is usually provided by using a battery and/or a solar panel, could be considered as a drawback of ARs. An ACR is able to provide a radar response seen as a bright pixel in the image and, possibly with a stable phase response. Historically, the use of transponders linked to spaceborne SAR has started since the first SAR space missions. They were mainly urged by the need of radiometric calibration, but also as tagging technique to identify and locate particular targets whose visibility is influenced by the surrounding environment. Recently, different companies have been involved in the manufacturing of ACRs, see Metasensing (2020) and Mahapatra et al. (2013), though their cost being expensive hinders their use at a larger extent by the wider community.

This document reports the design and the tests of ARs operating at 5.405 GHz ± 50 MHz. They are designed to be used in support of the spaceborne ESA Sentinel-1 SAR images processing and analysis. The developed ACRs is optimized at a cheaper price, with low power consumption, and to be portable with simple installation procedures.

2. DESIGN OF AN ACTIVE REFLECTOR

An AR consists of two antennas and an amplifying section, powered by a battery or any other available power source, see Figure 1. This section outlines the design of the AR implemented at CTTC, which works with Sentinel-1 data, see the technical details in Luzi et al. (2020).

A key parameter for the design is the Radar Cross Section, RCS, Skolnik (1990). This is given by the product of four terms, which are divided by $4 \cdot \pi$: (i) the gain of the amplifying section; (ii) the gain of the receiving antenna; (iii) the transmitting antenna gain; (iv) the square of the wavelength (Freeman et al., 1990). We assumed, as a requirement, a RCS greater than 40 dBsm. This value was fixed considering previous experience with PCRs. The gain of the two antennas was assumed to be greater than 15 dB.

A specific antenna was designed for our AR. A 4 by 4 linear patch array was designed to provide a gain value greater than 15 dB, hence reducing the necessary gain of the amplifying section, see Figure 2.

* Corresponding author

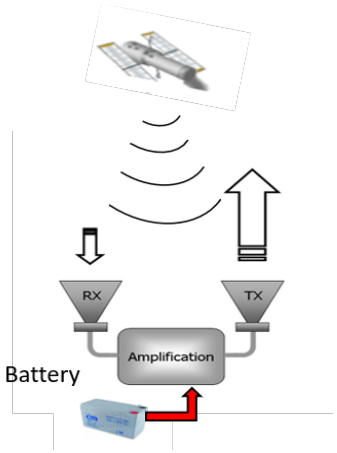

Figure 1. Scheme of the AR.

The AR amplifying section was built using off-the-shelf components. A market analysis was carried out to select some components considering their performances, costs and availability. The gain of the amplifying section was supposed to be not lower than 42 dB. The amplifying section needs to include a band-pass filter to reduce interferences coming from external sources, e.g. from wireless or mobile networks.

Figure 3 shows the scheme of the implemented AR. It includes: a low-noise amplifier (LNA) followed by a band-pass filter and four Medium Power Amplifiers (MPA). In addition, attenuators and isolators were added to reduce the saturation and optimize the line.

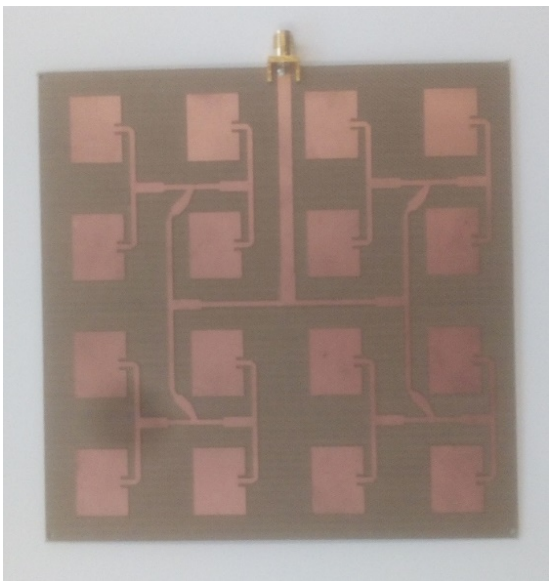

Figure 2. The patch array antenna (14 by 14 cm)

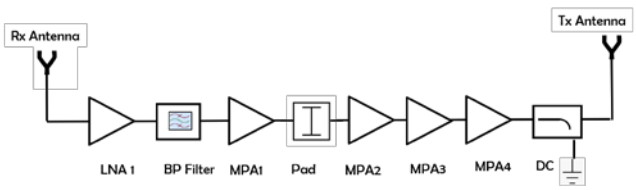

Figure 3. Scheme of the developed AR

3. EXPERIMENTAL RESULTS

3.1 Campus experiment

The first experiment was performed in the Campus of CTTC. Figure 4 shows the AR used in this experiment. The experiment consisted of the following steps:

1. In situ installation of a PCR and an AR; in addition, a Natural Corner Reflector (NCR) was also considered in the analysis.
2. Selection of pairs of Sentinel-1 images containing the AR and the PCR. The first image was acquired the 18 October 2019, and the last one the 16 January 2020.
3. Image co-registration and computation of the differential interferogram using pairs of temporally consecutive images. A total of 15 interferograms were analysed.
4. Phase unwrapping the interferograms.
5. Referencing all the phases to a given reference pixel.
6. Computing the temporally ordered phases, i.e. the phase time series. These phases are spatially referred to the reference point chosen in step. In addition, the phases are temporally referred to the first image, whose phase is set to zero.
7. The phase differences were transformed in displacements, expressed in [mm], see Figure 6.

Figure 5 shows a quick look of an image, displayed from the Sentinel Hub browser managed by ESA [8], corresponding to the area of interest. In this geocoded Sentinel-1 SAR amplitude the AR (ACR) the PCR (CR) and the Natural Corner Reflector (NCR) are clearly visible.

The displacement time series are shown in Figure 6. The time series of the PCR shows a slight (linear) trend up to approximately 6 mm: this is probably due to a settlement of this device. The most important result concerns the AR: it is basically stable. The deformation values range from -4.3 mm to +2.6 mm. The standard deviation of the deformation is 1.55 mm. Assuming that this is a stable point, this standard deviation is an experimental estimation of the phase stability of the AR. This is a reasonable phase stability performance.

Figure 4. AR prototype installed in the campus of CTTC

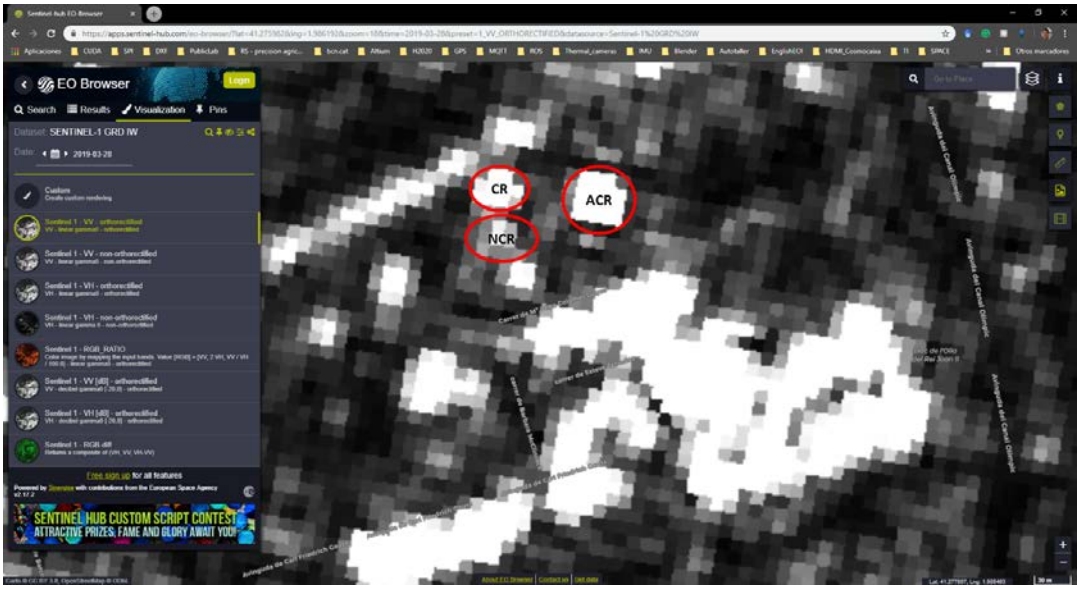

Figure 5. Amplitude Sentinel-1 image of the campus of CTTC. The red circles indicate the response of an AR (ACR), of a passive reflector (CR) and of a natural reflector (NCR)

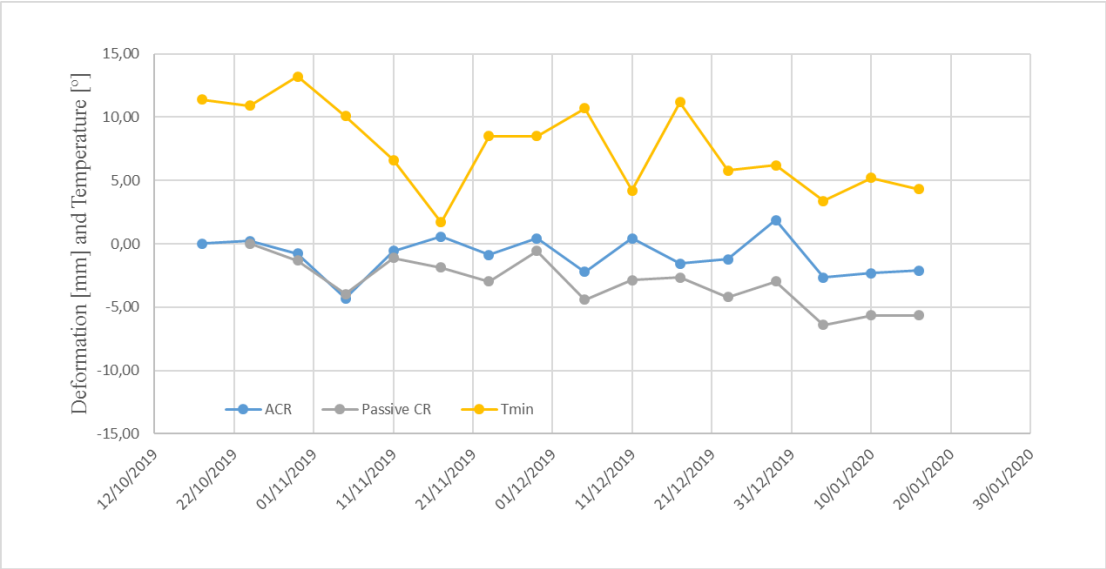

Figure 6. Deformation time series of an AR (ACR, blue line) and a PCR (grey line). Temperature of the acquisition dates of the used Sentinel-1 images (yellow line)

3.2 The Vipava (Slovenia) experiment – AR visibility

Two AR prototypes were installed in a Pilot Area of the EU H2020 GIMS project: the Vipava valley (Slovenia). The installation was performed on the 17, 18 and 19 June 2019. One of the two ARs (named AR1) was installed in a landslide area (see the Location 1 in Figures 8 and 9). The second AR (named AR2) was installed in the Location 2 (see Figure 8), close to the highway structure.

The first analysis concerned the visibility of the two ARs in the SAR images acquired starting from the 19th of June 2019 (i.e. after the AR installation). From the analysis of the first images, it was clear that the identification of the AR2 is difficult: the area of interest includes several bright SAR targets. Once a sufficient time series of SAR images was available, we were able to conclude that the AR2 response was not visible in the area of interest. The conclusion was that the ACR2 was not properly working.

The identification of AR targets in the Sentinel-1 SAR images is often a difficult task. This is mainly due to the medium resolution of these images, the presence of speckle noise, etc. An exception is given when a bright target (e.g. an AR or a PCR) is installed in an area of very low SAR amplitude. This is not the case in the area at hand. In fact, looking at the SAR amplitude images acquired after the AR installation, the AR1 is not clearly visible. Note that close to the AR1 location there are several other manmade objects that can respond strongly to the SAR signal. The result is that, in the corresponding SAR amplitude image, there are several bright reflectors in the area of interest.

Figure 7. GIMS Pilot Area 1: the Vipava valley (Slovenia). The AR1 was installed in the Location 1

Figure 8. The GIMS Pilot Area 1: the Vipava valley (Slovenia). Location of the AR1

The AR1 was identified by analysing the time series of 28 SAR amplitude images (from May 3 to September 30, 2019). We looked for pixels with strong amplitude value that were starting (right after) the data of the ACR1 installation.

We found three points as candidates. The first one shows a rather low response before the installation of the AR1. By contrast, starting from the AR1 installation, the amplitude is saturated at the maximum value. We believe that this pixel corresponds to AR1. The other two pixels are saturated after the AR1 installation. However, before this date they are characterized by rather high and variable amplitude values. These two pixels are affected by the AR1 installation, but they also include other responses coming from the neighbour manmade objects. In the following section, we only refer to the first pixel.

3.3 The Vipava (Slovenia) experiment – phase time series

The analysis of the phase time series involved the same steps used in the analysis of the campus (Section 3.1). Let's consider the pixel corresponding to the ACR1. Before referencing the phases to the reference point, given a date of the time series, the corresponding phase is the sum of the phase component due to the displacement of the target, the residual topographic error (RTE) phase component, the atmospheric phase component, and the phase noise.

Once the phases are referred to a given reference point R, they become the sum of the same component as above, but all the components contain phase differences: the phase difference between the displacement of the target and the one of the reference, the phase difference between the RTE of the target and the RTE of the reference, the phase difference between the atmospheric phase component of the target and the one of the reference, and finally the difference of the phase noises.

Under ideal conditions, the reference point is a strong target that has negligible noise, it is a stable point, it has the same RTE of the target and it is located relatively close to the pixel of interest in order to have the same atmospheric component of the target.

The analysis at hand is far from the above ideal conditions. It was carried out using as a reference point a natural target, whose phase noise component is unknown. In principle the other two terms (the one related to displacement and the one related to RTE) can be different from zero and not negligible. Finally, the atmospheric component (target versus reference) can be considered not negligible.

The displacement time series shown in Figure 10 is related to a reference point that is relatively close to the AR1 (see the location in Figure 9). It starts on the 20 June 2019 and ends on the 29 December 2019. The time series shows an almost linear trend, up to 9 mm at the end of the series.

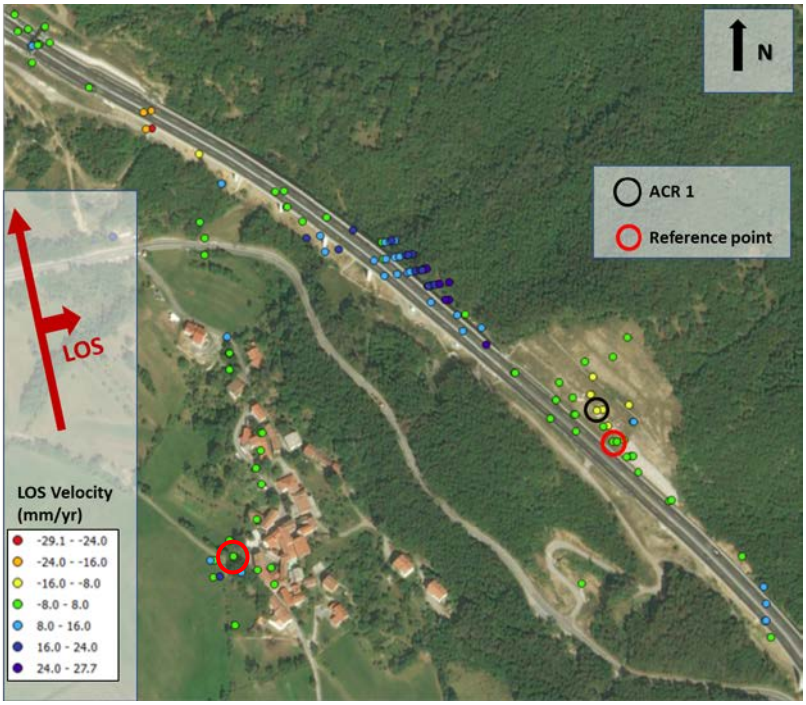

Figure 9. Location of the AR1 (black circle) and of the two reference points considered in this study (red circles)

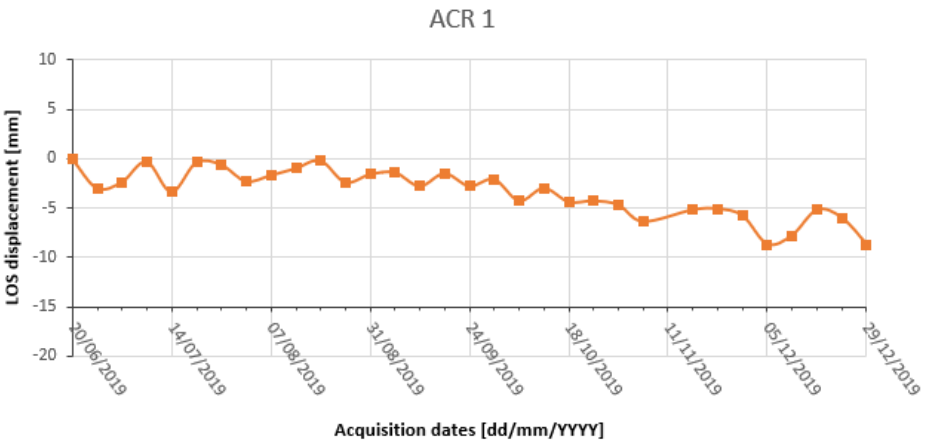

Figure 10. ACR1 displacement time series computed with respect to the reference point close to AR1

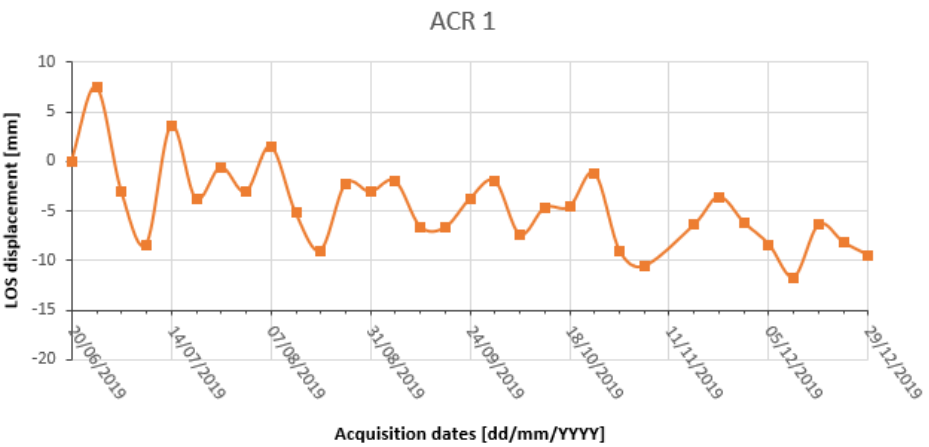

Figure 11. ACR1 displacement time series computed with respect to the reference point located in the bottom left side from Figure 9

The deformation time series related to the second reference point (see the location in the bottom left part of Figure 9) is shown in Figure 11. In this case the distance between the AR1 and the reference point is considerably larger than in the previous case.

The time series shows a general trend, which is approximately linear in time. The maximum displacement is approximately 10 mm (similar to the previous time series). The time series is considerably noisier than the previous one: the oscillations are probably due to the differential atmospheric effects between the analysed AR1 and the reference point.

4. CONCLUSIONS

The design and implementation of an AR, after several tests and improvements of the RF section, has been finally successful. In fact, the first goal to provide an adequate RCS has been achieved with a circuit based on low-cost radio frequency components. Another important component of the AR has been the design and implementation of a patch array antenna to be used for both signal reception and transmission.

In the experiment described in this paper, the visibility of the ARs in the SAR amplitude images has been demonstrated. Regarding the phase stability, the results obtained with an empirical approach, i.e. observing the behaviour directly on the deformation time series, has been promising. In particular, in the Campus experiment, a displacement standard deviation of 1.55 mm has been achieved.

This is a promising experimental result. It is worth noting that, due to the characteristics of the experiment, these values represent a rather pessimist estimation of the phase dispersion. In fact, the same standard deviation includes the other phase components, i.e. the one due to differential displacements (target versus reference point), to differential RTE and to differential atmospheric phase component. That is to say, the phase stability performance should be slightly better.

The next step is to make an accurate laboratory test to characterize the phase response of the device, evaluating the need of further improvements, which could involve different hardware aspects: thermal, electromagnetic and mechanical aspects. It is worth emphasising the need of an in-depth analysis to assess the AR phase stability as a function of the temperature. This is a critical aspect, to be further investigated.

ACKNOWLEDGEMENTS

This work is part of a project that has received funding from the European GNSS Agency under the European Union's Horizon 2020 research and innovation programme, with grant agreement No 776335, project GIMS, "Geodetic Integrated Monitoring System".

REFERENCES

Bamler, R., Hartl, P., 1998. Synthetic aperture radar interferometry. *Inverse Probl*, 14, R1-R54.

Crosetto, M., Gili, J.A., Monserrat, O., Cuevas-González, M., Corominas, J. and Serral, D., 2013. Interferometric SAR monitoring of the Vallcebre landslide (Spain) using corner reflectors. *Nat. Hazards Earth Syst. Sci*, 13(4), pp.923-933.

Freeman, A., Shen, Y. and Werner, C.L., 1990. Polarimetric SAR calibration experiment using active radar calibrators. *IEEE Transactions on Geoscience and Remote Sensing*, 28(2), pp.224-240.

Garthwaite, M., 2017. On the Design of Radar Corner Reflectors for Deformation Monitoring in Multi-Frequency InSAR. *Remote Sensing*, 9, 648.

Luzi, G., Espín Lóopez, P., Mira-Pérez, F., Monserrat, O., Crosetto, M., 2020. A low-cost Sentinel-1 Active Reflector designed to assist Interferometric Monitoring based on low cost benchmarking. Submitted to *IEEE Geoscience and Remote Sensing Letters*.

Mahapatra, P.S., Samiei-Esfahany, S., van der Marel, H. and Hanssen, R.F., 2013. On the use of transponders as coherent radar targets for SAR interferometry. *IEEE Transactions on geoscience and remote sensing*, 52(3), pp.1869-1878.

Metasensing website, 2020. http://www.metasensing.com/docs/MetaSensing-ecr-c.pdf.

Rosen, P.A., Hensley, S., Joughin, I.R., Li, F.K., Madsen, S.N., Rodriguez, E., Goldstein, R.M., 2000. Synthetic aperture radar interferometry. *Proceedings of the IEEE*, 88(3), 333-382.

Skolnik, M., 1990. *Radar Handbook*. Mc Graw Hill Publishing Company: New York, NY, USA, 1990.